14.3.   Two-dimensional Variational Analysis of Near-Surface Moisture from Simulated Radar Refractivity-related Phase Change Observations

Ken-ichi Shimose[1,3], Ming Xue[1,2*], Robert D. Palmer[2]
Jidong Gao[1], Boon Leng Cheong[2] and David J. Bodine[2]
[1]Center for Analysis and Prediction of Storms and [2]School of Meteorology
University of Oklahoma, Norman OK
[3]Department of Earth and Planetary Sciences
Kyushu University, Fukuoka Japan

1. Introduction

The amount and distribution of moisture are among the most important factors affecting the prediction of mesoscale and storm-scale weather (e.g., McPherson et al. 1997), particularly with regard to quantitative precipitation forecasting (Emanuel et al. 1995; Fritsch et al. 1998; Droegemeier et al. 2000). High-resolution measurements of moisture within the boundary layer (BL) are even more important because the BL moisture is the essential fuel for convection and precipitation.

Affected by often inhomogeneous lower boundary forcing and by BL physical processes involving, e.g., convective eddies and rolls, BL moisture has high spatial and temporal variability (Weckwerth et al. 1996; Weckwerth and Parsons 2006) but is poorly characterized by existing observing platforms (Weckwerth et al. 2004). Typical surface observation networks are too coarse to resolve the fine-scale structures. Furthermore, most remote sensing data, e.g., satellite measurements of water vapor in cloudy regions, are limited in regions of greatest interest.

Ground-based GPS receiver networks, while available in all weather conditions, provide only path-integrated quantities and lack resolution in the BL. In fact, the GPS-slant-path water vapor measurements are most effective at the mid to upper levels where slant paths intercept (Liu and Xue 2006). Therefore, high-resolution moisture measurements within the BL can fill the data gap and have the potential to significantly improve QPF.

It has been shown in recent years that high-resolution near-surface water vapor measurements can be derived from radar-based refractivity measurements utilizing returns from fixed ground targets (Fabry et al. 1997; Weckwerth et al. 2005). Effective assimilation of such observations into NWP model is an area that require significant amount of research. The actual impact of such ob-servations on storm-scale NWP also needs to be investigated, and this is most effectively done in collaboration with the instrumentation scientists, who in this case that radar engineers and radar meteorologists who have expertise in radar data processing starting from the signal processing level. Before testing data from a new platform, it is often valuable to perform experiments using simulated data, through Observing System Simulation Experiments (OSSEs, Lord et al. 1997) where observations as well as their error properties can be simulated and systematically evaluated.

In this paper, we describe an effort to develop a capability to analyze refractivity-derived measurement of near surface moisture based on the variational method, and we test such a capability using simulated refractivity and phase change data first. A previously modeled convective initiation case from the 2002 International H_2O Project (IHOP_2002) field experiment is chosen to serve as the truth. Simulated refractivity and phase change data are first created using a realistic radar simulator, and they are then analyzed using a specially designed 2DVAR system. The quality of the analysis is evaluated by comparing against the true moisture field.

The rest of this paper is organized as follows: section 2 describes background and generation of simulated radar phase change observations and section 3 introduces our 2DVAR analysis method. Results from analysis experiments are presented in section 4. Further discussions on the effectiveness of our scheme are given in section 5 through sensitivity experiments. Summary is given in section 6, together with a plan for future work.

2. Radar Refractivity and Phase Change Observations

a. Background

In vacuum, an electromagnetic wave travels at the speed of light ($c = 3 \times 10^8$ m s^{-1}). In the atmosphere,

---

* Corresponding author address: Ming Xue, CAPS, University of Oklahoma, 120 David Boren Blvd,

however, the wave is slowed by a factor equivalent to the index of refraction of the air, denoted by n. The refractivity, N, is a convenient term related to the refractive index and is defined by Bean and Dutton (1968),

$$N \equiv (n-1) \times 10^6 = 77.6 \left(\frac{P}{T} + 4810 \frac{P_w}{T^2} \right), \qquad (2.1)$$

where T is the temperature in degrees Kelvin, P is the total pressure and P_w is the partial pressure of water vapor. If there are no major changes in P and T, from (2.1), most of the spatial variability in N results from P_w (equivalent to water vapor).

An innovative technique was developed by Fabry et al. (1997). It is simple to show that the phase of the backscattered radar signal after coherent detection is related to the path-integrated refractive index by the following equation,

$$\phi(r,t) = \frac{4\pi f}{c} \int_0^r n(r',t) dr', \qquad (2.2)$$

where f is the radar transmitter frequency and r is the distance between the radar and ground clutter. As is evident from (2.2), the phase of the returned signal wraps around 2π approximately every half wavelength, which is 5 cm for an S-band radar, making the use of phase problematic for estimation of n. The original solution to the problem proposed by Fabry et al. (1997) is based on the use of a homogeneous reference observation. Reduction in phase wrapping is obtained by using the phase difference between a so-called reference time and the measured observation time (Fabry et al. 1997). The reference time should be chosen when the temperature and humidity fields could be assumed homogeneous over the field of view of the radar.

Given these two measurements of phase, the difference will be given by the following equation,

$$\begin{aligned} \Delta\phi(r) &= \phi(r,t_m) - \phi(r,t_{ref}) \\ &= \frac{4\pi f}{c} \int_0^r \left(n(r',t_m) - n(r',t_{ref}) \right) dr', \end{aligned} \qquad (2.3)$$

where $\phi_m(r)$ and $\phi_{ref}(r)$ denote the measured and reference phase values, respectively. An important point is that the phase will show a 2π-wrap less often since it is based on the refractive index difference. This difference will be much smaller than the

actual refractive index which is close to unity. Of course, the drawback is that we have to conduct the reference observations which are based on the homogeneity assumption. Nevertheless, the phase wrapping problem will be mitigated.

Again, we should emphasize that the refractive index change in (2.3), is integrated from the radar site to the target range. By taking the phase difference at two range values along the same radial where $R_2 > R_1$, we have

$$\begin{aligned} \Delta\phi(R_1, R_2) &= \Delta\phi(R_2) - \Delta\phi(R_1) \\ &\approx \frac{4\pi f}{c} \int_{R_1}^{R_2} \left(n(r',t_m) - n(r',t_{ref}) \right) dr' \end{aligned} \qquad (2.4)$$

Assuming the refractive index change is constant over the range from R_1 to R_2,

$$\begin{aligned} \Delta n(R_1, R_2) &= \Delta n(R_2) - \Delta n(R_1) \\ &= -\frac{c}{4\pi f} \frac{\Delta\phi(R_2) - \Delta\phi(R_1)}{R_2 - R_1} \end{aligned} \qquad (2.5)$$

where $\Delta n(R_i) = n(R_i, t_m) - n(R_i, t_{ref})$.

At this point, we have the refractive index change from the time of the reference observations. If the refractive index could be calculated from surface meteorological stations at the reference time, the actual value of n could be obtained.

Four major drawbacks exist with the original technique of Fabry et al. (1997):

(1) In order to mitigate the severe phase wrapping effect, the difference of a reference phase map with the measurement phase map was proposed. In addition to the logistically problems of obtaining a reference map, homogeneity assumptions over the observed field are not well justified under most conditions and certainly are difficult to validate.

(2) Complexity of the algorithm created numerous dependencies on individual radar platforms, reducing the overall impact of the technique on the meteorological community.

(3) Since the actual locations of the clutter targets are not known, it must be assumed that R_2 and R_1 are centered in their respective resolution volumes, which introduces a possibly significant error in the derivative operation in the final step of the algorithm (2.5).

(4) Measurements are limited to the near-surface.

Therefore, refractivity fields above the altitude of ground clutter targets cannot be estimated. Given the importance of moisture aloft for convective initiation, this is an important limitation.

If Δn field has a large gradient between R_1 and R_2, the phase wrapping occurs.

$$\Delta\phi(R_1, R_2) = \Delta\phi(R_2) - \Delta\phi(R_1) \geq 2\pi$$

Generally, the observable phase difference is mod($\Delta\phi(R_1,R_2)$, 2π). The phase wrapping is likely to occur, where the distance between two targets is larger, where there is a sharp gradient of refractivity difference between two targets and when the time difference between analysis and reference is larger In that case, we need special care for assimilating the phase difference between two targets. This issue is discussed in section 5.

b. Generation of simulated observations

Building on above knowledge, simulated refractivity and phase change data are created using a radar simulator for Observing System Simulation Experiments (OSSEs). The model used to produce the "true" field is the Advanced Regional Prediction System (ARPS, Xue et al. 2003) which is a nonhydrostatic atmospheric model formulated in a generalized terrain-following coordinate. Refractivity and phase change observations for OSSEs are created from a forecast from Xue and Martin (2006). This is for a dryline case that occurred on 24 May 2002 over the southern Great Plains of United States during the 2002 International H_2O Project (IHOP_2002) field experiment (Weckwerth et al. 2004). The ARPS model was initialized using analysis of the ARPS Data Analysis System (ADAS, Brewster 1996) at 1800 UTC 24 May 2002, and was integrated for 6 h. A 700 km $\times$ 400 km model domain at 1 km horizontal resolution was used (Fig. 1). For our simulation experiments, we assume that the surface fields from their simulation are located at a constant height surface, i.e., on a completely plat ground. These surface fields are used for the simulation of $\Delta\phi(R_1,R_2)$, which are considered the raw data.

An S-band radar ($\lambda = c/f \sim 0.1$ m) is assumed and placed on $x = 230$ km and $y = 350$ km of the domain shown in Fig. 1. For S-band radar, the detective range of N is within about 50 km radius of the radar.
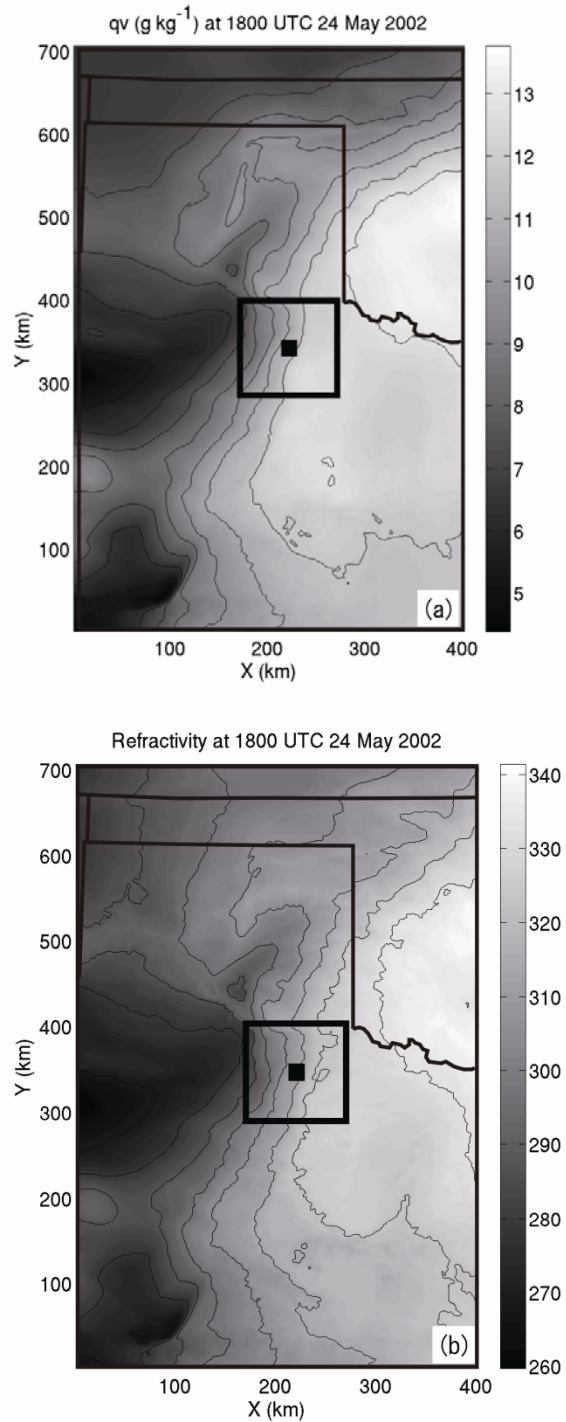

Figure 1: 2D fields of the water vapor (a), and simulated refractivity (b), at the surface at 1800 UTC 24 May 2002, the reference time. Black square mark denotes the radar location and open box denotes the area that is shown in Fig. 2.
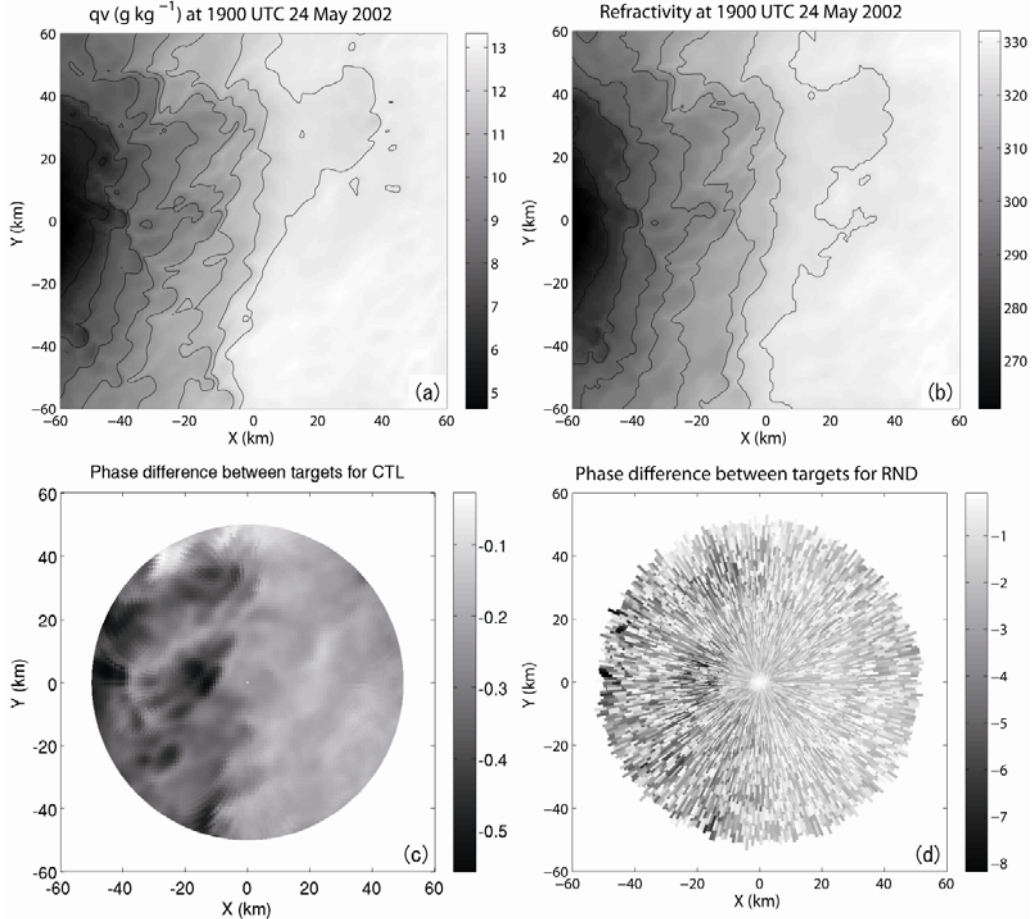
Figure 2: Simulated observations at the surface at 1900 UTC 24 May 2002, 1 hr after the reference time; (a) is the water vapor field, (b) is the N field, (c) is the phase difference between two targets for the case of uniform ground target case (hereafter CTL) and (d) is the phase difference for the case of for the case of random target distribution, RND (see Table 1).

Two types of ground target distributions are considered in this study:
(1) Uniform: Ground targets are distributed along the azimuth up to a 50 km range with uniform distances of 250 m, equaling the gate-spacing.
(2) Random: Ground targets are distributed along the azimuth from the radar to 50 km with random distances between 0.25 and 4 km.
In this study, the reference time is set at 1800 UTC 24 May 2002.

Figure 1a shows the water vapor field at 1800 UTC, the reference time. A distinct dry line is found from south to north. Figure 1b shows the simulated refractivity field, N, at the same time. N field has quite similar pattern as the q_v field because it is most sensitive to q_v. Often for forecasting purpose, N field is used as a reasonable proxy of q_v.

Figure 2 shows the q_v field and simulated N and phase change (between two ground targets) observations at 1900 UTC, 1 hr after the reference time. For the case of CTL, the distribution of the simulated

phase difference field is similar to the simulated N and none of the phase difference between two targets has been subject to phase wrapping ($-0.6 < \Delta\phi < 0$). For the case of RND, the phase difference is a function of the variable target difference so the pattern is none longer clear. In this case, phase wrapping often occurs where the distance between two targets is close to 4 km ($-8 < \Delta\phi < 0$). Although we should care about this phase wrapping issue, this matter is not considered in the case of RND, i.e., it is assumed that no phase wrapping has occurred even though in reality it should for some values. We discuss the issue of phase wrapped data in section 5.

3. Two-dimensional Variational Analysis Method

a. Methodology

In this work, a 2DVAR system is developed based on a univariate 3DVAR framework that was devel-

- 4 -

oped for analyzing GPS slant-path water vapor data that includes isotropic and anisotropic recursive filters (Liu and Xue 2006; Liu et al. 2007). In this study, surface water vapor field is analyzed by assimilating the phase differences between two targets, i.e., $\Delta\phi(R_1,R_2)$.

The cost function of our 2DVAR system is defined as

$$J\left(q_v^a\right) = J_b\left(q_v^a\right) + J_{phi}\left(q_v^a\right) \qquad (3.1)$$

where

$$J_b\left(q_v^a\right) = \frac{1}{2}\left(q_v^a - q_v^b\right)^T \mathbf{B}^{-1}\left(q_v^a - q_v^b\right) \qquad (3.2a)$$

$$J_{phi}\left(q_v^a\right) = \frac{1}{2}\left[H\left(q_v^a\right) - \Delta\varphi\right]^T \mathbf{R}^{-1}\left[H\left(q_v^a\right) - \Delta\varphi\right]. \qquad (3.2b)$$

In Eq. (3.1), cost function J is composed of background constraint term, J_b, and phase difference observation term, J_{phi}. q_v^a is the analysis value of the specific humidity q_v at the surface. The corresponding background state vector is q_v^b. The background term, J_b, measures the departure of the control variable from the background. Here $\mathbf{B}$ is the background error covariance matrix, which determines how the observational information is spread in space.

The phase difference observation term, J_{phi}, represents the departure of the analysis, calculated from q_v^a through the observational operator H, from the observations of the phase difference between two targets. The matrix $\mathbf{R}$ is the observation error covariance matrix for the phase difference between two targets, which is usually assumed to be diagonal under the assumption that observation errors are not correlated (some of the correlated errors can usually be effectively removed through bias correction procedures. see, e.g., Harris and Kelly 2001). In our paper, the magnitude of error variances or the diagonal elements of matrix $\mathbf{R}$ is much smaller than the background error variances and is specified.

The choice of spatial filter coefficients follow Liu and Xue (2006) and Liu et al. (2007). As mentioned earlier, the background error covariance controls the extent to which values at the grid points away from an observation are influenced by the observation.

For isotropic filter, the following Gaussian function can be used to model $\mathbf{B}$ (Huang 2000),

$$b_{ij} = \sigma_b^2 \exp\left[-\frac{1}{2}\left(\frac{r_{ij}}{L_r}\right)^2\right] \qquad (3.3)$$

where b_{ij} are the elements of $\mathbf{B}$, r_{ij} is the distance between two grid points i and j measured in terms of the grid index coordinate, L_r is the de-correlation length scale in terms of the grid intervals and is in practice often linked to the observation density. σ_b^2 is the background error variance, which we assumed to be calculated from the actual background error.

An alternative to Eq. (3.3) is the following anisotropic covariance (Horn and Johnson 1985, p.458 for Schur product theorem; Riishøjgaard 1998; Gaspari and Cohn 1999),

$$b_{ij} = \sigma_b^2 \exp\left[-\frac{1}{2}\left(\frac{r_{ij}}{L_r}\right)^2\right]\exp\left[-\frac{1}{2}\left(\frac{f_i - f_j}{L_f}\right)^2\right] \qquad (3.4)$$

where f is a field whose pattern represents that of the background error, which we call the error field. In this study, f is chosen to be either the true error field of the background or a certain estimate of the true error. L_f is the de-correlation scale in the error field space in units of g kg^{-1} for our analysis experiments; it controls the degree of the anisotropy.

b. Experimental design

In our experiments, 1800 UTC 24 May 2002 is chosen as the reference time for phase observations, and the moisture field is assumed known at this time. Three analysis times at 1900, 2100 and 2400 UTC are chosen to investigate the sensitivity of the analysis to time increment from the reference time. The larger is the increment, the more is chance the phase wrapping. At the analysis times, without any additional information, we assume the temperature and pressure are known and our goal is to analyze moisture from the phase change observations.

The ARPS model provides the mixing ratio of water vapor. The water vapor pressure needed in the refractivity formula can be derived using gas law

$$P_w = q_v \rho_d R_v T \qquad (3.5)$$

where ρ_d is the dry air density and R_v is the vapor gas constant. In our analysis, the reference refractivity field, N_{ref} is calculated from T, P, and q_v is set at 1800 UTC 24 May 2002, and q_v at 1800 UTC is used as the background value in the background term of the cost function. The background refractivity at each of the analysis times is calculated from q_v at 1800 UTC and the T and P from the analysis time, which are assumed known, as mentioned earlier.

4. Analysis experiments

To verify that the minimization procedure of our 2DVAR system works correctly, we first perform analysis experiments using phase difference data that contain no observational error, including phase wrapping. We mainly focus on the results at 1900 UTC 24 May 2002.

a. Single observation tests

To better understand the behaviors of 2DVAR system, two single observation experiments are performed first. This single observation is a phase difference between two targets of 2.75 km apart. The de-correlation scales L_r and L_f are specified as 3 km and 3 g kg^{-1}, respectively. The error level of the background is assumed very high in this case; in the final analysis is expected to fit the observation very closely.

Figure 3 shows the analysis increments from these two experiments. Because the observation is not a true point measurement, but an integrated quantity along a path, the analysis increment is isotropic filter exhibits a shape stretched in the direction of the path. The results of the anisotropic filter case (Fig. 3b) are similar. The analyzed peak values of the phase difference have the same value, -7.208, for both isotropic and anisotropic filter, which is very close to the observed value -7.217. Because the isotropic filter performs almost as well, especially when the observations have high resolutions (see later), the isotropic filter will be used in the control experiment.

b. Perfect observation experiments

The earlier single observation experiments demonstrate correct behaviors of our analysis system. Subsequently, we move to the analysis of the full 2D water vapor field from simulated phase difference observations. Two experiments are discussed in this section. In these two cases, simulated observations are 'perfect', the observations do not continued any errors. The variance of observational error is set as $2\pi/100$. De-correlation scale L_r and L_f are specified as 3 km and 3 g kg^{-1}, respectively. Sensitivity of the analysis to the value of the de-correlation scale is examined in next section. The first experiment is the control experiment, named CTL (Table 1); the distribution of the ground targets is uniform (see sec-

tion 2), and the 2DVAR uses isotropic recursive filter. Second experiment RND is the same as CNL, except that the data are 'Random' (Table 1).

Figure 4 shows the cost function and the norm of the cost-function gradient as functions the number of iterations during the minimization procedure for the experiment CTL. Significant reductions occur in both the cost function and the norm during the first 20 iterations. The cost function remains relatively flat afterwards while the gradient norm continues for decrease over the next 50 iterations or so. In all cases, we run the minimization algorithm for 100 iterations, which appear sufficient for the desired accuracy.

The analysis fields for CTL and RND at 1900 UTC 24 May 2004, 1 hr after the reference time, are shown in Fig. 5a and Fig. 5b, respectively. Both results are very close to the truth field where the observations exist (observations are confined to within the 50 km range). The root mean-square error (RMSE) and the maximum error (ME) between the analysis field and the true field are presented in Table 1. The RMSE and the ME are calculated inside of the radar detective range. The RMSE for CTL and RND are 0.032 g kg^{-1} and 0.037 g kg^{-1}, respectively, indicating good analysis. The ME for CTL and RND are 0.190 g kg^{-1} and 0.228 g kg^{-1}, respectively. For reference, the RMSE between the background field and the true field is 1.06 g kg^{-1}. Comparing the case of CTL with the case of RND, CTL has smaller error than RND because of the density of observation.

c. Sensitivity to de-correlation scale

The quality of an analysis is closely related to the de-correlation scales used in Eqs. (3.3) and (3.4); these scales control the spatial extent over which an observation increment is spread. Fixed values of L_r (3 km) are used in the earlier experiments. Anisotropic filter is not effective in this case so that only L_r is set as free parameter to determine the optimal L_r. We examine in this section how the analysis quality varies with the de-correlation scales, as measured by the RMSE between the analysis field and the true field.

Figure 6 shows the overall RMSE (g kg^{-1}) between retrieved analysis and true field, as a function of the de-correlation length L_r. For the perfect case (CTL and RND), we see that the optimal de-correlation length is equal to three grid intervals (3 km).
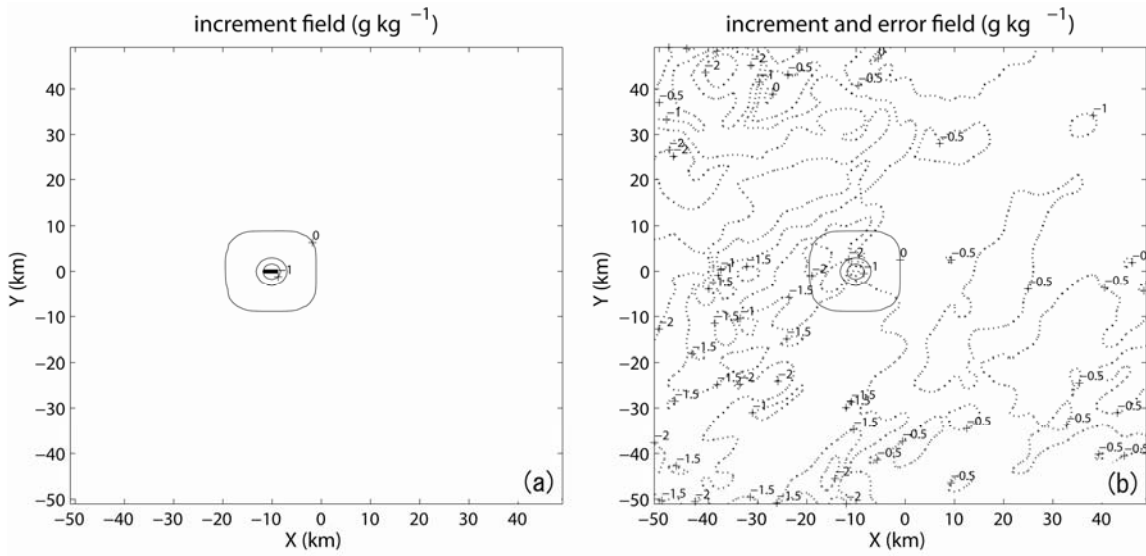
Figure 3: Analysis increments from single observation experiments; (a) is for the isotropic filter case and (b) for the anisotropic case. The dashed lines in (b) are the error field f in Eq. (3.4), taken as the truth – background here. The contour intervals are 0.5 g kg^{-1} for both fields. Black bold line denotes the path length between two targets 2.75 km apart.
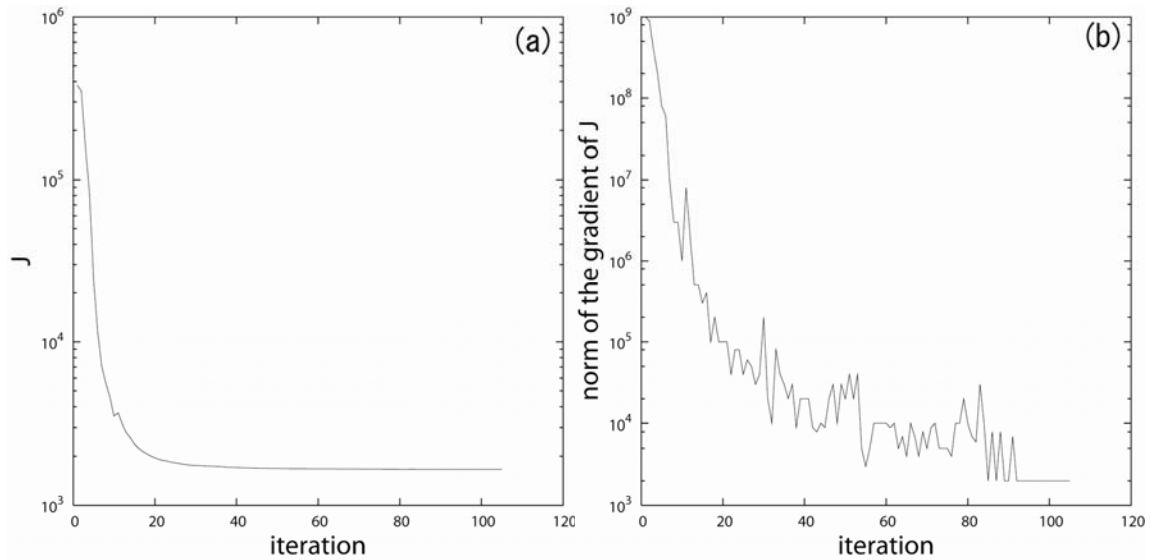
Figure 4: The variation of the cost function J, (a), and the norm of the gradient ∇J, (b), with the number of iterations during the minimization procedure for the case of CTL.
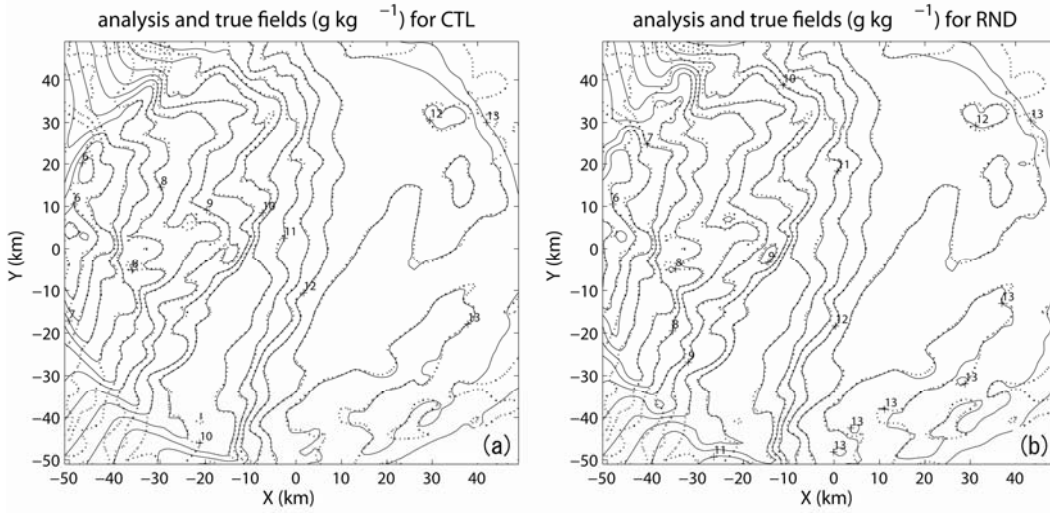
Figure 5: 2D analysis of water vapor fields (sold lines) at 1900 UTC 24 May 2002; (a) from CTL and (b) from RND. Dashed lines denote the truth field. The contour interval is 0.5 g kg⁻¹.

5. Sensitivity experiments

a. Sensitivity to target position errors

The radar used in this study is assumed S-band radar earlier. For S-band radar, the resolution of the radial direction is 250 m, this is the gate-spacing, so that we can not know the exact position of the ground target within the gate-grid. This ambiguity conducts the target position error because the actual measurement of the phase difference is from the actual target position, not from the gate. Hence, we should consider the target position error.

The added target position error is assumed as $r_{\text{target}} = r_{\text{gate}} \pm \alpha \, 250/2$ where α is a random number between -1 and 1 with uniform distribution. It is assumed that the phase difference observation, $\Delta\phi(r)$, is from r_{target} but it is valid at r_{gate}. Following analysis experiments, we perform experiments CTL_PE and RND_PE, which are the same as experiments CTL and RND except for the errors added to the targets.

The analysis of CTL_PE and RND_PE are shown in Table 1. The RMSE for CTL_PE and RND_PE are 0.039 g kg⁻¹ and 0.036 g kg⁻¹, respectively, and the ME for CTL_PE and RND_PE are 0.421 g kg⁻¹ and 0.222 g kg⁻¹, respectively. The ME for both cases are increased by adding the target position error. The RMSE for both cases, however, scarcely change. The sensitivity to the de-correlation scale for CTL_PE and RND_PE are shown in Fig. 6. The

optimal de-correlation length is the same as the perfect case and the tendency of the RMSE value is similar to the perfect case. From these results, the target position error doesn't affect the analysis significantly.

b. Sensitivity to observational errors

All experiments presented so far are not considered the observational error. In practice, the observations would not be error-free, so it is important to test the sensitivity of the analysis to the observational errors, in part to test the robustness. The standard deviations added the simulate observations is 5, 10, 15 and 20 % of the error free values and the added errors are normally distributed with zero means. We perform experiments CTL_OE and RND_OE, which are the same as experiments CTL and RND except for 10 % errors added to the observations, and CTL_POE and RND_POE, which are the same as CTL_PE and RND_PE except for 10 % errors.

The analysis of CTL_OE, RND_OE, CTL_POE and RND_POE are shown in Table 1. The RMSE for CTL_OE, RND_OE, CTL_POE and RND_POE are 0.045 g kg⁻¹, 0.110 g kg⁻¹, 0.065 g kg⁻¹ and 0.111 g kg⁻¹ respectively. The RMSE for RND_OE and RND_POE are increased significantly. The RMSE for CTL_POE is greater than that of CTL_OE, but their value are still small. Figure 7 shows the analysis fields for CTL_POE and RND_POE at 1900 UTC 24 May 2004. We can see that both analysis

- 8 -

fields are still close to the true field even though the observational errors are added. Figure 8 shows the RMSE between analysis and true field as a function of the percentage of observational errors for experiments CTL_OE, RND_OE, CTL_POE and RND_POE. For cases of CTL_OE and CTL_POE, the observational error does not affect significantly, while, for cases of RND_OE and RND_POE, the RMSE exhibits larger increase with the amount of error. However, the RMSE for RND_OE and RND_POE are still small and keep valid value.

c. Sensitivity to the phase wrapping

All experiments presented so far are not considering the phase wrapping. In the actual observation, however, the phase wrapping occurs as shown in Fig. 2d. The phase wrapping is likely to occur, where the distance between two targets is larger, where there is a sharp gradient of refractivity difference between two targets and when the time difference between analysis and reference is larger.

In our experiments, the case of RND only has this issue. To include this issue, we perform experiment RND_MOD, which is the same as RND except that the original simulated phase difference observation is divided by 2π and that remainder is taken as the new simulated observation.

Figure 9a shows the analysis field for RND_MOD at 1900 UTC 24 May 2004. We can see that the analysis field exhibits quite large value where the phase wrapping occurs (see Fig. 2d). From Table 1, the RMSE and the ME for RND_MOD are 0.411 g kg^{-1} and 4.876 g kg^{-1}, respectively. Especially, the ME for RND_MOD is quite large so that our system is completely collapsed where the phase wrapping occurs.

To defeat the issue of the phase wrapping, we perform the experiment UNW, which is the same as RND except for applied the 'unwrapping' process which follows the same way as the actual observational process by Cheong et al. (2007). In the unwrapping process, the original simulated phase difference observation are spatially interpolated into every gate spacing and smoothed to get rid of the phase wrapping. Figure 9b shows the analysis field for UNW at 1900 UTC 24 May 2002. We can see that the quite large values in Fig. 9a are improved. Because of the smoothing process, it seems that the analysis field is also smoothed. However, the RMSE and the ME for UNW are 0.141 g kg^{-1} and 0.999 g kg^{-1}, respectively, indicating valid analysis. The sen-

sitivity to the de-correlation scale for UNW and UNW_PE, which is the same as UNW except for added position errors, are shown in Fig. 6. The optimal de-correlation length is equal to eight grid intervals (8 km); this value is different from experiments CTL and RND. It is because that the original simulated observation is interpolated and smoothed spatially. Figure 12a shows the analysis field for the experiment UNW_POE, which is the same as UNW_PE except for added observational errors. The analysis field seems to be smoothed but still to be close to the true field. The RMSE and the ME for UNW_POE, 0.152 g kg^{-1} and 0.946 g kg^{-1}, respectively, still indicating valid analysis. From these results, our system defeats the issue of the phase wrapping. Furthermore, although the experiment UNW_POE includes all errors, the analysis field keeps valid information. So our system is valid to analyze the water vapor field from the phase change observation.
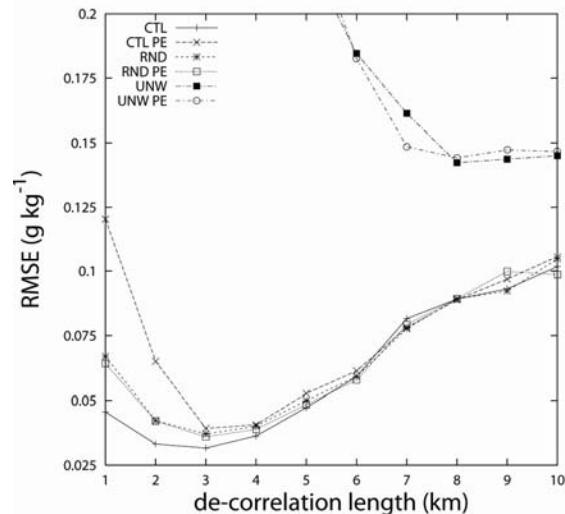

Figure 6: The overall RMSE (g kg^{-1}) between analysis and truth field, as a function of the de-correlation length L_r.

d. Sensitivity to the time evolution

All experiments presented so far used the simulated observations at 1900 UTC 24 May 2002, 1 hr after the reference time. To investigate the sensitivity to the time evolution of the weather system, we performed experiments UNW_POE at 2100 UTC and 2400 UTC, 3 hrs and 6 hrs after the reference time. The analysis fields for UNW_POE at 2100 UTC and 2400 UTC are shown in Fig. 10b and 10c. By these times, the model simulations have devel-

oped fine-scale boundary layer convective eddies and rolls, and convection was initiated along the dryline around 2100 UTC, the moisture fields exhibit much more small scale structures than at 1900 UTC. For this reason, the moisture field analysis RMSE are somewhat larger, at 0.421 g kg^{-1} and 0.272 g kg^{-1}, respectively (Table 1). Fig. 10b and c show that the analyzed contours still match those of the truth reasonably well. In these two cases, the background q_v used in the cost function is obviously more different from the truth at these times than that at 1900 UTC.

Figure 8: The overall RMSE (g kg^{-1}) between analysis and truth field as a function of the percentage of error.

6. Conclusions

A 2DVAR analysis system is developed for analyzing the 2D water vapor near the surface from radar refractivity-related phase change observations. Such observations can be obtained by an innovative technique initially developed by Fabry et al. (1997); the phase of the backscattered radar signal after coherent detection is related to the path-integrated refractive index, which is strongly linked to water vapor, from the radar to ground targets. In our simulation experiments, uniformly and non-uniformly spaced ground targets are considered. An ARPS simulation of a convective initiation case, serving at the 'truth' is sampled using the radar simulator to produce realistic refractivity-related phase deference observations between ground targets.

Our 2DVAR analysis system is based on a 3DVAR framework of Liu et al (2007) that includes isotropic and anisotropic recursive filter options. 2DVAR analysis experiments are conducted using the simulated observations and the quality of the analyses is evaluated through comparisons with the true field. The results are summarized as follows.
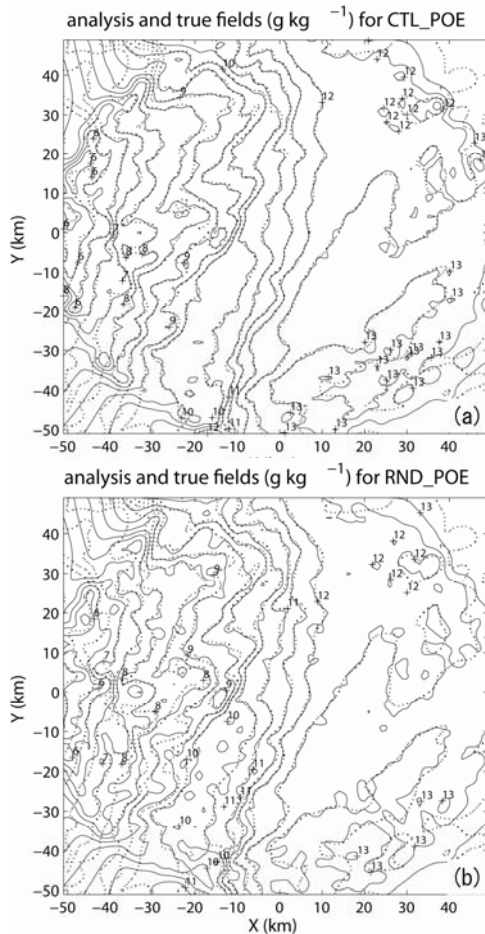

Figure 7: 2D analysis of water vapor fields (sold lines) at 1900 UTC 24 May 2002; (a) from CTL_POE and (b) from RND_POE, both with 10 % observational error. Dashed lines denote the truth field. The contour interval is 0.5 g kg^{-1}.
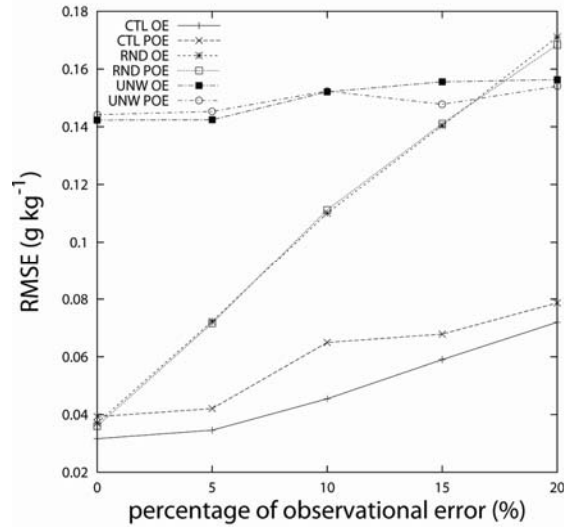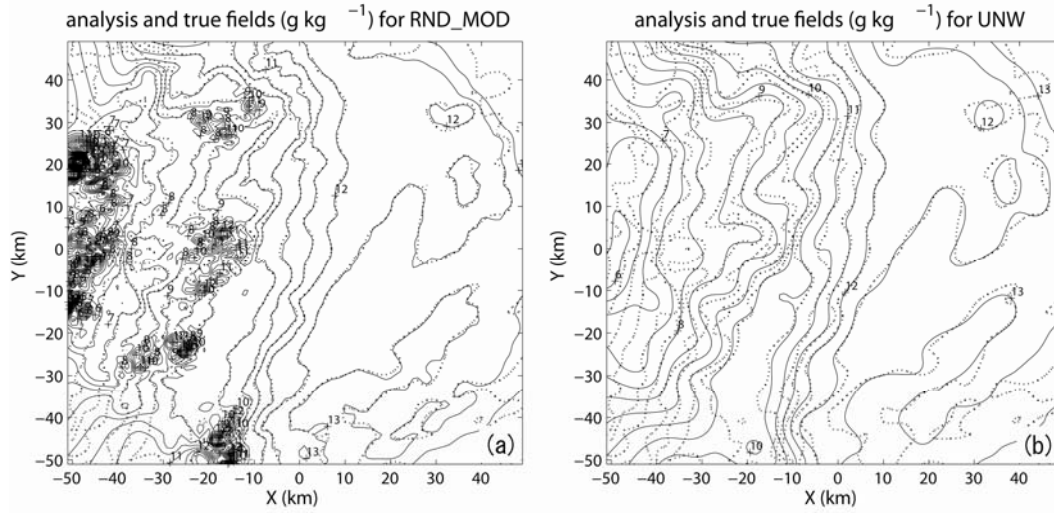
Figure 9: 2D analysis of the water vapor fields (sold lines) at 1900 UTC 24 May 2002; (a) from RND_MOD and (b) from UNW. Dashed lines denote the truth field. The contour interval is 0.5 g kg^{-1}.

Table 1: List of experiments. For experiments, MOD: considering the phase wrapping, PE: added position errors, OE: added observational errors and POE: added both position errors and observational errors. For Distributions, Uniform: targets distributed every 250 m on one azimuth, Random: targets distributed between 250 m and 4 km randomly on one azimuth, Unwrapped: targets distributed randomly but interpolated every gate spacing and the phase difference is unwrapped. RMSE is the root-mean square error between the analysis moisture and the true moisture and Max Error is the maximum absolute error value between analysis and true moisture. RMSE between true and background moisture at 1900, 2100 and 2400 UTC 24 May 2002 are 1.06, 2.32 and 1.75 g kg^{-1}, respectively.

| Experiments	Target distribution	Position Errors ($\pm$ 125 m)	Obs. Errors (10 %)	RMSE (g kg^{-1})	Max Error (g kg^{-1})
CTL	Uniform	No	No	0.032	0.190
CTL_PE	Uniform	Yes	No	0.039	0.421
CTL_OE	Uniform	No	Yes	0.045	0.243
CTL_POE	Uniform	Yes	Yes	0.065	0.395
RND	Random	No	No	0.037	0.228
RND_PE	Random	Yes	No	0.036	0.222
RND_OE	Random	No	Yes	0.110	0.745
RND_POE	Random	Yes	Yes	0.111	0.631
RND_MOD	Random	No	No	0.411	4.876
UNW	Unwrapped	No	No	0.142	0.999
UNW_PE	Unwrapped	Yes	No	0.144	0.832
UNW_OE	Unwrapped	No	Yes	0.152	1.040
UNW_POE	Unwrapped	Yes	Yes	0.152	0.946
UNW_POE 2100 UTC	Unwrapped	Yes	Yes	0.421	2.381
UNW_POE 2400 UTC	Unwrapped	Yes	Yes	0.272	2.251
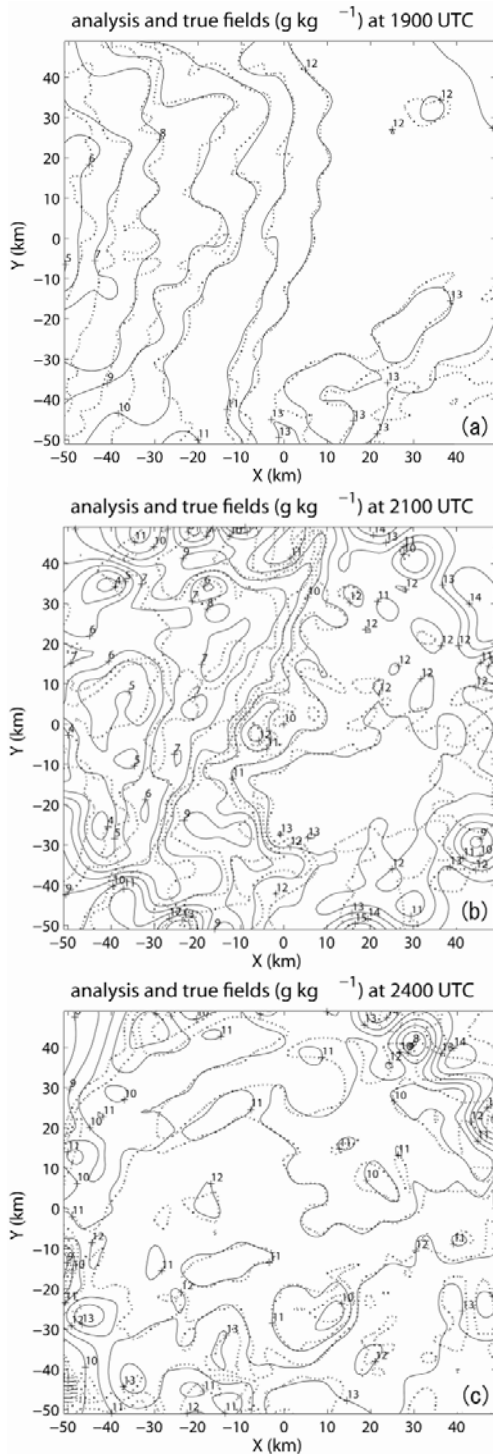
Figure 10: 2DVAR analysis of the water vapor fields (sold lines) from UNW_POE; (a) at 1900 UTC, (b) at 2100 UTC and (c) at 2400 UTC 24 May 2002. Dashed lines denote the truth field. The contour interval is 1.0 g kg^{-1}.

1) The moisture field analysis produced by our 2DVAR system with an isotropic recursive filter captures the detail structure of moisture field.

2) Experiments on the sensitivities of the analysis to target position ambiguity (uncertain within one range gate) errors show that such error does not affect the analysis significantly.

3) Experiments on the sensitivities to observational errors are performed. For cases of uniform ground target distributions, it is found that the observational error does not affect analyses significantly, while, for cases of random distributions, the analyses become worse with the increase in observational errors. Still, the analyses remain generally valid.

4) Our 2DVAR system fails when the observations include the phase wrapping. When the data are first unwrapped in a separate processing step, the analysis can succeed. In the unwrapping process, involves spatial interpolation and smoothing of the original phase different data therefore the analyzed moisture field is smoother.

In our current analysis system, the moisture field is the only variable and temperature and pressure fields are assumed to be known. In the future, we will use multi-variate assimilation methods such as the ensemble Kalman filter (EnKF, Evensen 2003; Evensen 2006) where moisture, temperature and pressure fields will be analyzed simultaneously.

References

Bean, B. R. and E. J. Dutton, 1968: Radio Meteorology. *Dover Publications*, 435.

Brewster, K., 1996: Application of a Bratseth analysis scheme including Doppler radar data. *Preprints, 15th Conf. Wea. Anal. Forecasting*, Norfolk, VA, Amer. Meteor. Soc., 92-95.

Droegemeier, K. K., J. D. Smith, S. Businger, C. I. Doswell, J. Doyle, C. Duffy, E. Foufoula-Georgiou, T. Graziano, L. D. James, V. Krajewski, M. LeMone, D. Lettenmaier, C. Mass, R. S. Pielke, P. Ray, S. Rutledge, J. Schaake, and

E. Zipser, 2000: Hydrological Aspects of Weather Prediction and Flood Warnings: Report of the Ninth Prospectus Development Team of the U.S. Weather Research Program. *Bull. Amer. Meteor. Soc.*, **81,** 2665-2680.

Emanuel, K., D. Raymond, A. Betts, L. Bosart, C. Bretherton, K. Droegemeier, B. Farrell, J. M. Fritsch, R. Houze, M. LeMone, D. Lilly, R. Rotunno, M. Shapiro, R. Smith, and T. A, 1995: Report of the first Prospectus Development Team of the U.S. Weather Research Program to NOAA and the NSF. *Bull. Amer. Meteor. Soc.*, **76,** 1194-1208.

Evensen, G., 2003: The ensemble Kalman filter: Theoretical formulation and practical implementation. *Ocean Dynamics*, **53,** 343-367.

Evensen, G., 2006: *Data Assimilation: The Ensemble Kalman Filter*. Springer, 280 pp.

Fabry, F., C. Frush, I. Zawadzki, and A. Kilambi, 1997: On the extraction of near-surface index of refraction using radar phase measurements from ground targets. *J. Atmos. Oceanic Technol.*, **14,** 978-987.

Fritsch, J. M., R. A. J. Houze, R. Adler, H. Bluestein, L. Bosart, J. Brown, F. Carr, C. Davis, R. H. Johnson, N. Junker, Y.-H. Kuo, S. Rutledge, J. Smith, Z. Toth, J. W. Wilson, E. Zipser, and D. Zrnic, 1998: Quantitative precipitation forecasting: Report of the eighth prospectus development team, U.S. Weather Research Program. *Bull. Amer. Meteor. Soc.*, **79,** 285-299.

Gaspari, G. and S. E. Cohn, 1999: Construction of correlation functions in two and three dimensions. *Quart. J. Roy. Meteor. Soc.*, **125,** 723-757.

Harris, B. A. and G. Kelly, 2001: A satellite radiance-bias correction scheme for data assimilation. *Quarterly Journal- Royal Meteorological Society*, **127,** 1453-1468.

Horn, R. A. and C. R. Johnson, 1985: *Matrix analysis*. Cambridge University Press, 561 pp.

Huang, X.-Y., 2000: Variational analysis using spatial filters. *Mon. Wea. Rev.*, **128,** 2588–2600.

Liu, H. and M. Xue, 2006: Retrieval of moisture from slant-path water vapor observations of a hypothetical GPS network using a three-dimensional variational scheme with anisotropic background error. *Mon. Wea. Rev.*, **134,** 933–949.

Liu, H., M. Xue, R. J. Purser, and D. F. Parrish, 2007: Retrieval of moisture from simulated GPS slant-path water vapor observations using 3DVAR with anisotropic recursive filters. *Mon. Wea. Rev.*, **135,** 1506–1521.

Lord, S. J., E. Kalnay, R. Daley, G. D. Emmitt, and R. Atlas, 1997: Using OSSEs in the design of the future generation of integrated observing systems. *Preprint volume, 1st Symposium on Integrated Observation Systems*, Long Beach, CA, Amer. Meteor. Soc., 45-47.

McPherson, R., E. Kalnay, and S. Lord, 1997: The potential role of GPS/MET observations in operational numerical weather prediction. The Global Positioning System for the Geosciences, NRC Rep. 9254. National Academy Press [Available online at http://www.nap.edu/catalog/9254.html], 111-113.

Riishøjgaard, L. P., 1998: A direct way of specifying flow-dependent background error correlations for meteorological analysis systems. *Tellus*, **50A,** 42-57.

Weckwerth, T. M. and D. B. Parsons, 2006: A review of convection initiation and motivation for IHOP_2002. *Mon. Wea. Rev.*, **134,** 5–22.

Weckwerth, T. M., J. W. Wilson, and R. M. Wakimoto, 1996: Thermodynamic variability within the convective boundary layer due to horizontal convective rolls. *Mon. Wea. Rev.*, **124,** 769–784.

Weckwerth, T. M., C. R. Pettet, F. Fabry, S. Park, M. A. LeMone, and J. W. Wilson, 2005: Radar refractivity retrieval: Validation and application to short-term forecasting. *J. Appl. Meteorol.*, **44,** 285-277.

Weckwerth, T. M., D. B. Parsons, S. E. Koch, J. A. Moore, M. A. LeMone, B. B. Demoz, C. Flamant, B. Geerts, J. Wang, and W. F. Feltz, 2004: An overview of the International H2O Project (IHOP_2002) and some preliminary highlights. *Bull. Amer. Meteor. Soc.*, **85,** 253-277.

Xue, M. and W. J. Martin, 2006: A high-resolution modeling study of the 24 May 2002 case during IHOP. Part I: Numerical simulation and general evolution of the dryline and convection. *Mon. Wea. Rev.*, **134,** 149–171.

Xue, M., D.-H. Wang, J.-D. Gao, K. Brewster, and K. K. Droegemeier, 2003: The Advanced Regional Prediction System (ARPS), storm-scale numerical weather prediction and data assimilation. *Meteor. Atmos. Physics*, **82,** 139-170.